SAND2020-8971C

Evaluation of Probing Signals for Implementing Moving Horizon Inertia Estimation in Microgrids

Manisha Rauniyar†, Sterling Berg, Sunil Subedi
Timothy M. Hansen, Robert Fourney, Reinaldo Tonkoski
South Dakota State University
Brookings, South Dakota, USA
Email: †manisha.rauniyar@jacks.sdstate.edu

Ujjwol Tamrakar
Sandia National Laboratories
Albuquerque, New Mexico, USA

***Abstract*—This paper investigates existing probing signals for accurate estimation of inertia and damping constants in microgrids. Increasing utilization of renewable energy sources and their different dynamics has created unknowns in time-varying system inertia and damping constants. Thus, it is difficult to know these parameters at any given time in converter-dominated microgrids. This paper describes the design characteristics, considerations, methodology, and accuracy level of different probing signals in determining unknown parameters of a system. The main goal of this paper is to find an effective probing signal with a simple implementation and minimal impacts on power system operation. The test-case model in this paper analyzes non-intrusive excitation signals to perturb a power system model (i.e., square wave, multisine wave, filtered white Gaussian noise, and pseudo-random binary sequence). A moving horizon estimation (MHE)-based approach is then implemented in an energy storage system (ESS) in MATLAB/Simulink for estimation of inertia and damping constants of a system based on frequency measurements from a local phase-locked-loop (PLL). The accuracy of parameter estimates alters depending on the chosen probing signal; when estimating inertia and damping constants using MHE with the different probing signals, square waves yielded the lowest error.**

***Index Terms*—Energy storage systems, probing signals, inertia estimation, microgrids, moving horizon estimation.**

I. Introduction

Increasing implementation of converter-based renewable energy sources (RESs) is leading to a reduction in the power system inertia. Low-inertia systems are more susceptible to changes in load/generation that lead to a large rate of change of frequency (ROCOF) [1]. The inertia of a power system is traditionally estimated based on the number of online synchronous generators. However, RESs such as photovoltaic solar and wind typically do not add inertia as they replace traditional synchronous generators, causing the system inertia to vary over time [2]. The stochastic nature of RESs makes estimating the inertia of a power system more challenging. Additionally, converters with virtual inertia control algorithms can be used to connect RESs to benefit system stability, further compounding the inertia estimation process [3]. Under uncertain inertia estimates, deployment of fast-frequency control/support strategies can be challenging.

Traditionally, inertia estimation has been performed using offline methods, such as a polynomial approximation technique applied to a frequency transient waveform [4], *after* the transient has occurred. Offline approaches to inertia estimation may not be useful for real-time adaptive control techniques as the true inertia value may change over time. Methods for real-time online inertia and damping constant estimation have been developed in [5], [6]. However, these approaches may not be always available in microgrids [7]. Based on the frequency transient measurements, the inertia constant of the system has been estimated in [8], but the damping constant was not considered in this approach. It becomes computationally expensive to extract the inertia constant value based on the ambient frequency measurements using a system identification approach [6]. An estimation technique that uses local measurements is preferable for a wider range of applications, such as microgrids. Moving horizon estimation (MHE) was recently shown as a viable approach to provide real-time inertia and damping constant estimation using local measurements from a phased-locked loop (PLL) of an energy storage system (ESS) [7]. In [7], a MHE-based approach was proposed to estimate the inertia and damping constant of microgrid system based on perturbation from ESSs. The microgrid was perturbed using a low-level square wave power signal from an ESS, and the system response was analyzed using MHE to estimate the inertia and damping constants. Online parameter estimation often involves the use of an excitation signal. The design of these signals has been investigated for online power system identification and closed-loop inertia estimation based on PMU measurements in [5], [9]. MHE for estimating microgrid parameters is a new approach, and the efficacy of this implementation depends on the excitation signals employed. This paper evaluates the performance MHE using different excitation signals reported in the literature for online estimation of power system inertia and damping constants.

This work is supported by the U.S. Department of Energy under grant number DE-SC0020281, National Science Foundation (NSF) MRI-1726964 and OAC-1924302, and the SDSU Research, Scholarship and Creative Activity Challenge Fund. This research made use of the "Roaring Thunder" cluster at South Dakota State University funded under NSF grant number CNS-01726946.

The authors would like to thank Dr. Imre Gyuk, Director of Energy Storage Research, Office of Electricity for his funding and guidance on this research.

Sandia National Laboratories is a multi-mission laboratory managed and operated by National Technology and Engineering Solutions of Sandia, LLC., a wholly owned subsidiary of Honeywell International, Inc., for the U.S. Department of Energy National Nuclear Security Administration under contract DE-NA-0003525. This paper describes objective technical results and analysis. Any subjective views or opinions that might be expressed in the paper do not necessarily represent the views of the U.S. Department of Energy or the United States Government.

978-1-7281-8192-9/21/$31.00 ©2021 IEEE.

The paper is organized as follows: Section II introduces the basic concept of MHE. Section III discusses the characteristics of various probing signals. The design procedure of excitation signals and simulation setup is explained in Section IV, followed by the results and analysis in Section V. Finally, the conclusions are provided in Section VI.

II. Basic Concept of MHE

MHE is a finite horizon optimization based estimation process that is used to infer state variables and parameters of a system from its measurements. In this approach, one uses measurements of the plant, plant model, and inputs to estimate the plant states and parameters in the presence of unmeasured disturbances and measurement noise [10]. Fig. 1 illustrates the basic concept of MHE, where N represents the length of the estimation horizon window, T_s represents the estimator sampling time, the crosses represent the measured outputs (possibly noisy) from the MHE model, and the solid line with circles is the estimated values taken from the system. The output of the system is represented by y_k at discrete time instant k. Once the data is collected for a fixed length of N, the current process states and parameters are estimated in each sampling time by solving an online optimization problem that minimizing the error between the measurements and predictions of the states from the plant model. In the subsequent sampling instances, the horizon moves forward, but the length of the horizon window remains constant at N.

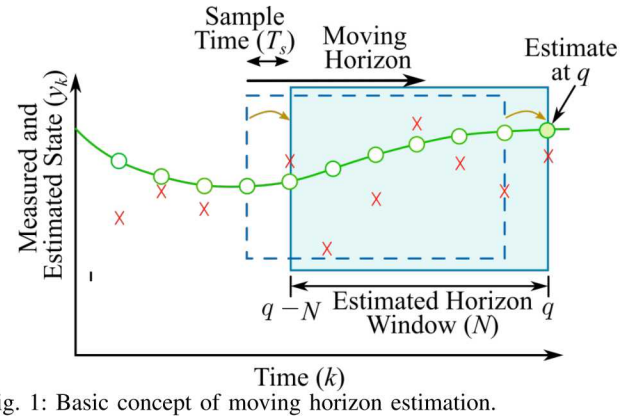

Fig. 1: Basic concept of moving horizon estimation.

III. Probing Signal Characteristics and Design Considerations

The objective of probing signal design is to create an excitation signal that gives accurate estimates of states and parameters of system, while minimizing impact on the operation of the power system and energy medium. The choice of probing signals has a substantial influence on the estimated data, which will be shown in Section V. A number of important design factors need to be considered while designing a probing signal, described in detail for traditional approaches in [5], [9]. To minimize the impact on the power system and the ESS lifetime, probing signals with sharp transitions and high ramp rates may need to be avoided. The peak amplitude of the probing signal should be small when probing for a long duration, and often must be limited to prevent damage [9]. In this paper, the efficacy and characteristics of four probing signals are investigated: 1) Multisine Wave, 2) Ramp-limited Square Wave, 3) Filtered White Gaussian Noise (FWGN), and 4) Pseudo-Random Binary Signal (PRBS).

A. Multisine Wave Probing Signal

A multisine signal is composed of the sum of multiple sinusoids:

$$x(t) = \sum_{i=1}^{N} A_i cos(\omega_i t + \theta_i) \tag{1}$$

The frequency spectrum of a multisine signal can be designed by selecting the sinusoidal component amplitudes, A_i, and frequencies, ω_i, that compose the signal, $x(t)$, where θ_i represents the phases of each component.

Signals with higher amplitudes and higher signal-to-noise ratio (SNR) provide better system parameter estimates in both traditional and MHE approaches [7], [9]. However, because the peak amplitude of the probing signal often needs to be limited to minimize the power system impact, it is desirable to minimize the crest factor of the signal for a higher SNR. The crest factor (C_r) of a signal is defined as the ratio between the peak value V_{pk} and the RMS value V_{RMS} [11]. Minimizing the crest factor increases the amount of the signal that is above a given noise floor. For example, if a square wave ($C_r = 1$) and sine wave ($C_r = \sqrt{2}$) have the same peak amplitude, the square wave will have a higher average magnitude than the sine wave. The crest factor of multisine waves can be reduced using the method described in [11].

The period of the multisine wave T is another important consideration, because the resolution of component frequencies $\Delta f = \frac{1}{T}$ is directly related to the period of the multisine wave. Longer periods require longer tests and may make averaging results more difficult, but will increase the resolution of frequency domain analysis [9].

B. Square Wave Signal

Square waves are a simple signal to generate from an ESS inverter and have a crest factor $C_r = 1$. However, the high ramp rates of square waves may be detrimental to the lifetime of different ESSs. In addition, restrictions from power conversion systems can create additional challenges to implement the signal. Using a ramp-limited square wave is an option for reducing the impact on ESSs, however decreasing the ramp-rate of a square wave will increase the crest factor and possibly affect the peak amplitude, potentially reducing estimation accuracy.

C. FWGN and PRBS Signal

For periodic signals, such as the multisine and ramp-limited square waves, a specific group of frequencies are excited by a single signal. To excite a higher number of frequencies, a non-periodic signal, such as FWGN or PRBS, can be used. The spectral energy of the FWGN can be manipulated by the type of filter used on the noise. The energy of a PRBS

can be concentrated in a desired frequency band using similar techniques. Design of these signals is described in more detail in Section IV-A.

IV. Methodology

A. Design of Excitation Test Signals

The excitation signals were designed using a method similar to that described in [5], [9]. The multisine wave was optimized by placing sinusoidal components in the frequency band of interest and minimizing the crest factor. Fig. 2 shows a flowchart for the design of the multisine wave. First, 100 random multisine waves based on (1), were generated using frequencies in the band of interest (0.1-0.5Hz) with randomized amplitudes and phases. This frequency band corresponds to a typical inertial constant range of $2-10$ s [12], which must be adequately excited for identification [9]. The multisine wave with the lowest crest factor was selected from the randomly generated multisine waves. Then, an algorithm similar to that described in [11] was applied to this multisine wave to further reduce the crest factor.

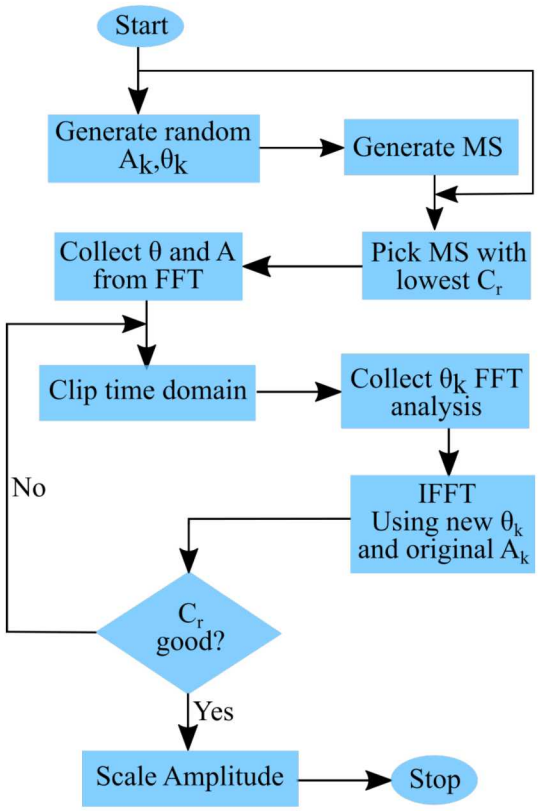

Fig. 2: Flowchart representing the design of multisine wave signal.

The algorithm used to minimize crest factor while still maintaining a multisine shape is shown in Fig. 2 [11]. First, the Fast Fourier Transform (FFT) was performed on the original waveform and the amplitudes and phases were recorded. Next, the time domain waveform was clipped to 75% of the peak magnitude. After clipping, another FFT was performed on the clipped signal and the new phases were recorded. Then, a new

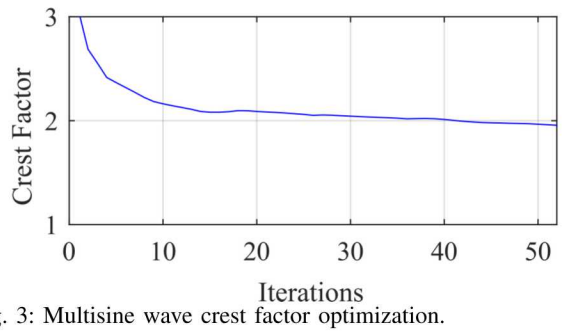

Fig. 3: Multisine wave crest factor optimization.

time domain signal was constructed by applying an inverse FFT (IFFT), using the original amplitudes and the phases of the clipped signal. This process was repeated 50 times, or until the crest factor no longer significantly decreased. Fig. 3 shows the results of an application of the algorithm from [11] where the crest factor was reduced from 3.05 to 1.85. The time domain plot of the multisine signal used is shown in Fig. 4.

The FWGN signal, shown in Fig. 4(b), was generated by filtering white Gaussian noise with a bandpass filter. The noise was generated using the $wgn()$ function in MATLAB [13], and was filtered using a minimum-order bandpass filter with a stop band attenuation of 60 dB [13]. The PRBS signal, Fig. 4(c), was created by ceiling and flooring the positive and negative values of the FWGN signal to the desired amplitude, allowing for the frequency spectrum of the PRBS to be manipulated. Finally, the square waves were generated with amplitudes varying from 0.02-0.2 p.u. and ramp rates ranging from 0.5-5 p.u. per second. Ramp-limited square waves with ramp rates lower than 0.5 p.u./s yielded high error in estimation and were not considered for comparison and analysis. A sample square wave signal is shown in Fig. 4(d).

The different distributions of energy can be seen in the frequency spectrums of the four different excitation signals in Fig. 5. The signals were designed such that the energy would be concentrated in the frequency band of interest (0.1-0.5 Hz). The multisine wave and FWGN signals have a large percentage of their total energy concentrated in that band, 98% and 97%, respectively. PRBS and the square wave signals also have comparative percentages of energy in the band of interest, 38% and 23%, respectively. In theory, the signal will be more efficient if the energy is limited to the frequency range of interest [5].

B. MHE and Simulation Setup

The isolated power system model described in [14] is used in this paper to test the MHE with designed excitation signals. The simulation setup in MATLAB/Simulink implemented with MHE is shown in Fig. 6. The simulation parameters for the equivalent generator model are given in Table I. The probing signals designed in Section IV-A are used as the excitation signals to perturb the frequency and ROCOF of the system. The online measurements of frequency and ROCOF are likely to contain noise, assuming they are made from a PLL of an ESS. To make the measurements more realistic, white

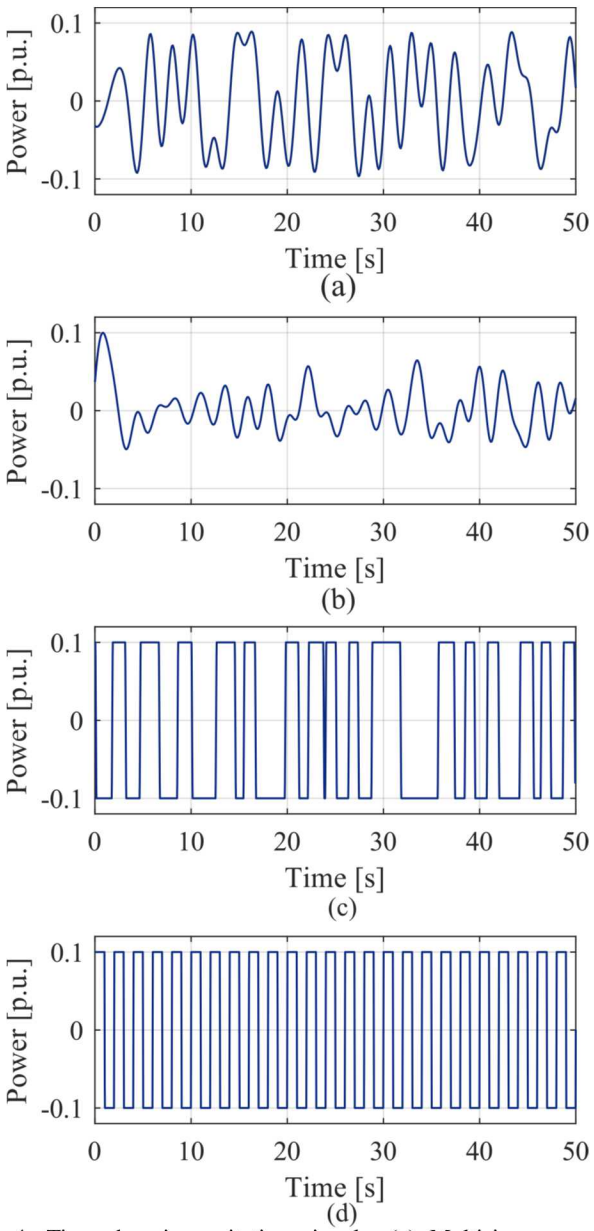

Fig. 4: Time domain excitation signals: (a) Multisine wave. (b) FWGN. (c) PRBS. and (d) Square wave.

Gaussian noise was added to model frequency measurements with a covariance of 10^{-7} and SNR of 60 dB, which is typical for PLL measurements [15]. The MHE uses measurements at each sampling instant to estimate the inertia and damping constant of the power system model.

TABLE I: Summary of Simulation Parameters

Parameter	Values
Inertia constant (M)	10 s
Damping coefficient (D)	1.5%
Speed regulation droop (R_p)	5%
Turbine-Governor time constant (T_g)	0.5 s
Sample time	0.02 s

In [7], the following estimation algorithm was presented to

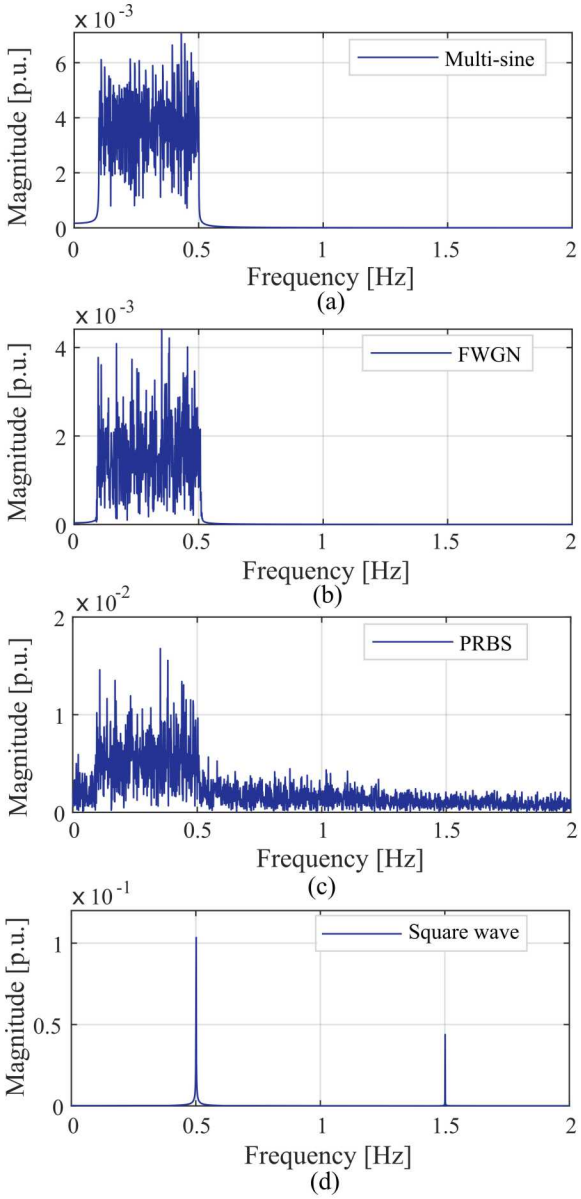

Fig. 5: Frequency spectrum of the excitation signals.

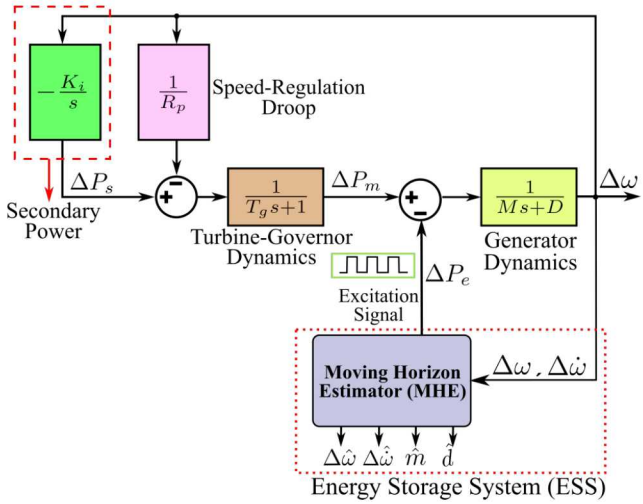

Fig. 6: Simulation setup for parameter estimation using different excitation signals.

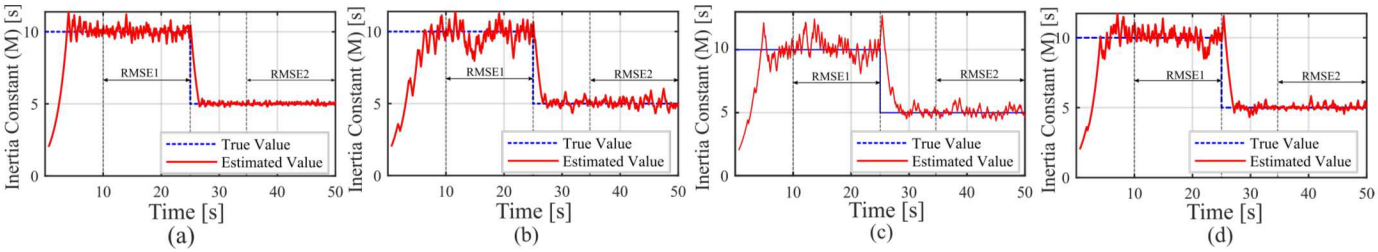

Fig. 7: Estimation of inertia constants. (a) Square wave. (b) Multisine wave. (c) FWGN. (d) PRBS.

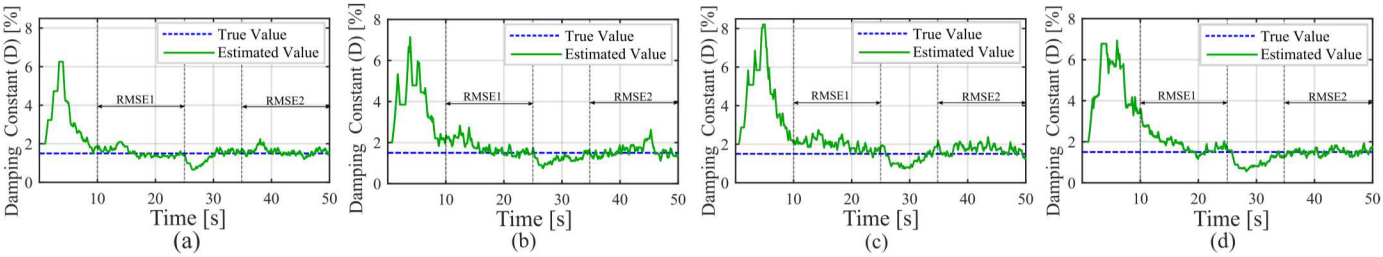

Fig. 8: Estimation of damping constants. (a) Square wave. (b) Multisine wave. (c) FWGN. (d) PRBS.

estimate the inertia and damping constant using MHE:

1) Set time horizon and sampling time;
2) Take frequency and ROCOF measurements at sampling times;
3) Collect N data points for the measurement matrix;
4) Guess an initial state and parameter;
5) Estimate states and parameters by MHE;
6) Remove the oldest measurement and append the newest measurement; and
7) Use the last estimate as an initial guess for upcoming iterations.

The MHE was implemented with an estimation horizon $N = 30$ and sampling time $T_s = 0.02$ s. More details regarding the implementation are available in [7]. In this paper, we focus on investigating the effect using the design excitation signals on the performance of the MHE.

V. Results and Analysis

The results of inertia and damping constant estimates for various excitation signals can be seen in Figs. 7 and 8, respectively. The true value of system inertia constant is initially set to 10 s, which changes to 5 s at a simulation time of 25 s. The damping constant is kept constant at 1.5% throughout the simulation. The accuracy in parameter estimation is illustrated by performing two different test cases on the Simulink model and comparing the RMSE values from the different excitation signals. RMSE values for inertia and damping constants are estimated for different time instants of the simulation. The RMSE calculation is done when the parameters are in steady state. In the first case (RMSE1), the RMSE estimation is performed from time instant $t = 10$ s to 25 s. Similarly, the RMSE was calculated from time instant $t = 35$ s to 50 s for the second test case (RMSE2). RMSE1 and RMSE2 in Figs. 7 and 8 represent the measurement window used for calculating RMSE. The RMSE for different excitation signals are compared in Fig. 9.

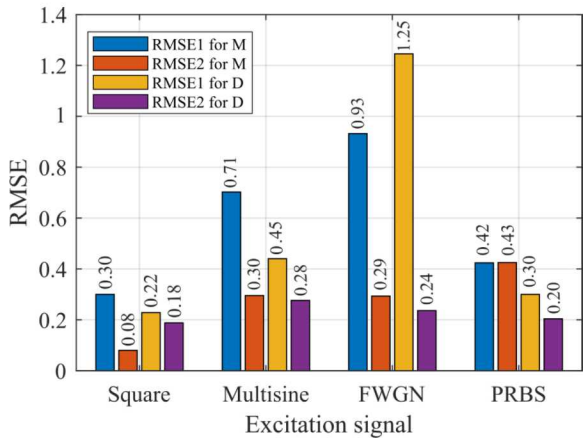

Fig. 9: Comparison of RMSE when estimating true values of M and D for different excitation signals.

The stochastic, non-periodic signals (i.e., FWGN and PRBS) yielded relatively poor estimation results. The high crest factor of FWGN likely explains why it performed worse than the multisine wave. This does not explain the large difference in performance between PRBS and square wave excitation signals. PBRS and square waves have similar time domain shapes and percentages of spectral energy in the band of interest as square waves. However, the square wave signal has higher amplitude frequency components than the PRBS signal that may enable a better estimation even in the presence of measurement noise.

The MHE performed well with the multisine excitation signal. The multisine estimation had a higher error while estimating when the inertia constant was 10 s compared to the case when the inertia constant was 5 s. This is because when

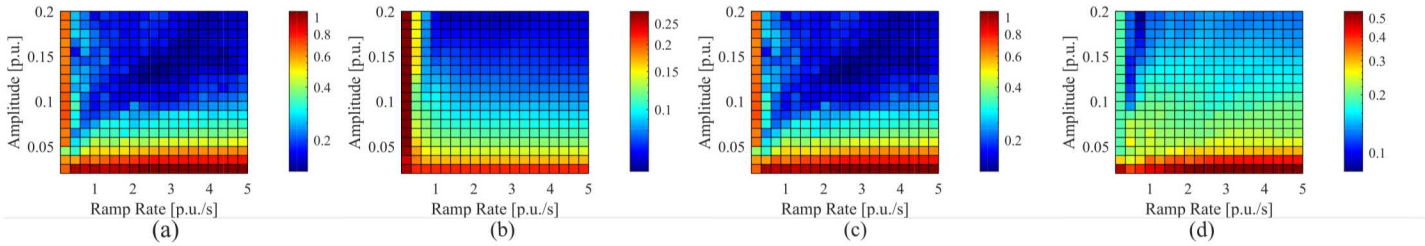

Fig. 10: Heat maps showing effect of varying square wave ramprate and amplitude on RMSE (logarithmic scaling, blue is better; note the different color scale). Estimating (a) M from 10 – 25 s. (b) M from 35 – 50 s. (c) D from 10 – 25 s. (d) D from 35 – 50 s.

the true inertia constant is lower, the same excitation signal leads to higher changes in system frequency and ROCOF. Based on the observations from the different excitation signals, the square wave signal had the highest accuracy for inertia and damping estimation. However, other considerations like the amplitude, ramp rate, higher frequency component amplitude, and difficulty of implementation should be considered when choosing an excitation signal.

To observe the impact on estimation accuracy, a sweep of amplitude and ramp rate of the square waves was performed. Amplitude was varied in the range of [0.02, 0.2] and the ramp rate was varied in the range of [0.1, 5]; each with 20 data points. The results were summarized in Fig. 10 using heat-maps, where lower (i.e., blue) is better for variations in RMSE values of inertia and damping constant estimation.

Higher amplitude excitation signals produced better estimation results due to higher SNR as can be observed from Fig. 10. For the simulated measurement noise with covariance of 10^{-7}, if the amplitude of the excitation signal was less than approximately 0.05 p.u., the accuracy of estimation decreased significantly. As long as the peak amplitude was not affected by limiting the ramp rate, ramp-limited square waves still showed high accuracy. This suggests that for a given amplitude and frequency, the ramp rate may be limited to preserve the lifetime of ESS and reduce the impact on the system without negatively affecting the accuracy of MHE.

VI. Conclusions

The objective of this research was to evaluate low-level excitation signals that result in accurate MHE of inertia and damping constants without affecting the power system operation and limiting the impacts on the ESS. The characteristics and design considerations of the probing signals were discussed from the perspective of power system identification theory. The accuracy of parameter estimates alters depending on the chosen probing signal and signal parameters. When estimating inertia and damping constant using MHE with different perturbation methods (i.e., square wave, multisine, FWGN, and PRBS signals), square waves yielded the lowest RMSE. The ramp rate of a square wave excitation signal can be limited without significantly reducing its effectiveness. It may be computationally expensive or difficult to generate the other signals in the ESS inverter to meet all requirements. Furthermore, the square wave has a higher frequency component amplitude in the signal in comparison with the PRBS signal. Thus, the resulting RMSE was found to be the best for the square wave perturbation method, however, the impact on frequency deviations and ROCOF has not been considered and is part of our future work.

Acknowledgments

The authors would like to thank Dr. Rodrigo Trevizan, Sandia National Laboratories for reviewing the technical content of this paper. The authors would also like to thank Mr. Niranjan Bhujel and Mr. Abodh Poudyal for their valuable technical input.

References

[1] F. Milano, F. Dörfler, G. Hug, D. J. Hill, and G. Verbič, "Foundations and challenges of low-inertia systems (invited paper)," in *2018 Power Systems Computation Conference (PSCC)*, 2018, pp. 1–25.

[2] ERCOT, "Inertia: Basic concepts and impacts on the ERCOT grid," *ERCOT, Tech. Rep.*, 2018.

[3] U. Tamrakar, D. Shrestha, M. Maharjan, B. Bhattarai, T. Hansen, and R. Tonkoski, "Virtual inertia: Current trends and future directions," *Applied Sciences*, vol. 7, p. 654, 2017.

[4] T. Inoue, H. Taniguchi, Y. Ikeguchi, and K. Yoshida, "Estimation of power system inertia constant and capacity of spinning-reserve support generators using measured frequency transients," *IEEE Transactions on Power Systems*, vol. 12, no. 1, pp. 136–143, 1997.

[5] J. Zhang and H. Xu, "Online identification of power system equivalent inertia constant," *IEEE Transactions on Industrial Electronics*, vol. 64, no. 10, pp. 8098–8107, 2017.

[6] K. Tuttelberg, J. Kilter, D. Wilson, and K. Uhlen, "Estimation of power system inertia from ambient wide area measurements," *IEEE Transactions on Power Systems*, vol. 33, no. 6, pp. 7249–7257, 2018.

[7] U. Tamrakar, "Optimization-based fast-frequency support in low inertia power systems," Ph.D. dissertation, South Dakota State University, 2020.

[8] T. Inoue, H. Taniguchi, Y. Ikeguchi, and K. Yoshida, "Estimation of power system inertia constant and capacity of spinning-reserve support generators using measured frequency transients," *IEEE Transactions on Power Systems*, vol. 12, no. 1, pp. 136–143, 1997.

[9] J. W. Pierre, N. Zhou, F. K. Tuffner, J. F. Hauer, D. J. Trudnowski, and W. A. Mittelstadt, "Probing signal design for power system identification," *IEEE Transactions on Power Systems*, vol. 25, no. 2, pp. 835–843, 2010.

[10] N. Hashemian and A. Armaou, "Fast moving horizon estimation of nonlinear processes via carleman linearization," in *2015 American Control Conference (ACC)*, 2015, pp. 3379–3385.

[11] E. Van der Ouderaa, J. Schoukens, and J. Renneboog, "Peak factor minimization using a time-frequency domain swapping algorithm," *IEEE Transactions on Instrumentation and Measurement*, vol. 37, no. 1, pp. 145–147, 1988.

[12] P. Kundur, N. J. Balu, and M. G. Lauby, *Power system stability and control*. McGraw-Hill New York, 1994, vol. 7.

[13] Generate white gaussian noise samples. [Online]. Available: https://www.mathworks.com/help/comm/ref/wgn.html

[14] U. Tamrakar, T. M. Hansen, R. Tonkoski, and D. A. Copp, "Model predictive frequency control of low inertia microgrids," in *2019 IEEE 28th International Symposium on Industrial Electronics (ISIE)*, 2019, pp. 2111–2116.

[15] S. Wang, J. Zhao, Z. Huang, and R. Diao, "Assessing gaussian assumption of PMU measurement error using field data," *IEEE Transactions on Power Delivery*, vol. 33, no. 6, pp. 3233–3236, 2017.